

Contents lists available at ScienceDirect

Polymer

journal homepage: www.elsevier.com/locate/polymer





Interplay of photopolymerization and phase separation kinetics and the resulting structure-property relationship of photocurable resins

Lauren Zakrzewski ^a, Yeongsik Kim ^a, Younghan Song ^a, Chang Y. Ryu ^a, Chulsung Bae ^a, Catalin R. Picu ^{b,*}

- ^a Department of Chemistry and Chemical Biology, Rensselaer Polytechnic Institute, Troy, NY, 12180, USA
- ^b Department of Mechanical, Aerospace and Nuclear Engineering, Rensselaer Polytechnic Institute, Troy, NY, 12180, USA

ARTICLE INFO

Keywords: Photo-PIPS Phase separation Thermosets

ABSTRACT

In this work we develop thermoset materials with heterogeneous microstructures on sub-micron scales by photopolymerization-induced phase separation (photo-PIPS). To this end, we designed a photo-curable resin based on pentaerythritol tetraacrylate (PETA), an acrylate monomer, combined with 2-ethylhexyl methacrylate (2-EHMA), a methacrylate diluent. Polypropylene glycol (PPG) was used as a phase separation agent. Phase separation was monitored by reactive light transmittance using a custom-built light transmission apparatus and through dynamic mechanical analysis (DMA). The photopolymerization kinetics and the microstructure morphology were characterized using real-time Fourier transform infrared spectroscopy (FTIR) and scanning electron microscopy (SEM), respectively. We observe double phase separation: PETA and 2-EHMA separate due to different reactivities, while PPG phase separates as the network develops due to immiscibility. A synergy is observed between the two processes: PPG phase separation leads to an enhanced separation of 2-EHMA. Phase separation leads to reduced transmittance due to scattering, which is primarily associated with the separation of 2-EHMA. Phase separation also causes the reduction of stiffness due to the formation of PPG subdomains. The kinetics is enhanced by increasing the PPG molecular weight and increasing the irradiation intensity.

1. Introduction

Controlling the structure of polymeric networks is a growing pursuit in the field of material science for its broad applications, ranging from polymer membranes for fuel cells to liquid polymer crystals for optical displays [1-23]. Producing materials with diverse morphologies is of particular interest as it can replicate similar enhanced properties to naturally occurring, heterogeneous materials [24-30]. Several approaches have been explored for this purpose, such as block copolymer self-assembly, polymer blends, and polymerization-induced phase separation (PIPS) [31–39]. For block copolymer self-assembly, the reaction and processing conditions need to be carefully controlled and the preparation of each individual block needs to be done with a high degree of precision [16,31,32]. In the case of polymer blends, it is difficult to control the degree of heterogeneity as mixing often introduces various constraints on the ability to blend [33-39]. The viscosities of each polymer used, the method of mixing, and the time or rate used to mix the polymers all affect the degree of network heterogeneity [16,33-39].

Compared to polymer blends and block copolymer self-assembly, PIPS produces phase-separated structures without such strict processing constraints [1,2,9,11,13–16,18–21,40–47].

PIPS begins with an initially homogeneous, liquid multicomponent monomer resin [1,2,15,16,40–47]. Upon polymerization, an immiscible component present in the multicomponent mixture phase separates, forming its own subdomains and creating a heterogeneous material [40–47]. In the PIPS process, phase separation occurs due to the thermodynamic driving force captured in the Flory-Huggins equation,

$$\frac{\Delta G_{mix}}{nRT} = \frac{\varphi_A \ln \varphi_A}{N_A} + \frac{\varphi_B \ln \varphi_B}{N_B} + \chi \varphi_A \varphi_B, \tag{1}$$

where n is the total number of molecules, N_x and φ_x are the degree of polymerization and volume fraction of each component [1–3,48–50]. The first two terms relate to the entropy of the process and the last term relates to the enthalpy. As polymerization of one component occurs, entropy changes. Specific chemistries cause differences in χ , and increasing χ indicates greater immiscibility. The degree of phase

^{*} Corresponding author.

E-mail address: picuc@rpi.edu (C.R. Picu).

separation also depends on the kinetics of the process which is controlled by the diffusion of the molecules. In solutions of reactive oligomers and linear chains of the phase-separating component, as used in this work, the oligomer diffusion is fast, and kinetics of phase separation is conditioned by the formation of the network. Systems that reach complete phase separation are those which have attained thermodynamic equilibrium. In all other cases, the constituent phases remain partly mixed, and the structure is defined by the rate of polymerization.

PIPS may proceed through various reaction types including cation, anion, and even radical photopolymerization (photo-PIPS) [1–3,5–11, 13–23,40–47]. Among them, photo-PIPS is the most desirable as it could be used in various applications including stereolithography 3D printing, which is a high-resolution printing technique that has grown in popularity in recent years [45,51–53].

To induce photo-PIPS in thermosetting materials, a multicomponent liquid comprised of monomer(s), a photoinitiator, and an additive which induces phase separation upon monomer polymerization is used [2,15, 16,18,19,42,44–46]. Various immiscible species such as a polymer or nanoparticles may be used as phase-separating additives. The resulting phase separation creates a complex nano- and/or microstructure which affects the material mechanical properties, such as enhancing the strength and/or ductility. Alternately, the phase-separated additives may be removed using solvents or pyrolysis to yield a structure with nanoscale porosity [40,45,54]. This method offers additional opportunities to adjust and control the overall mechanical properties.

There are (at least) three main challenges with PIPS: i) controlling the morphology (subdomain sizes, bicontinuous structures, etc.), ii) controlling the properties of the interfaces between separating phases, and iii) controlling the internal stress state [3]. To adjust the morphology and subdomain size, the chain length of the polymer additives, or the size and concentration of nanoparticles, can be modified [15,16,38,39]. The interfacial properties may be adjusted using block copolymers [3]. The residual stress depends on the type of polymerization and degree of defectiveness of the resulting network.

Herein we study photo-PIPS in a system that exhibits two phase separation processes. We use a photo-curable diacrylate resin with a methacrylate diluent and polypropylene glycol (PPG) as the phaseseparating additive. The resin and diluent tend to phase separate due to their different polymerization rates, while the additive PPG drives additional phase separation. We observe a synergy between the two processes, i.e. both phase separation processes become more pronounced as the driving force for PPG separation increases. The kinetics of photopolymerization is monitored by measuring the rates of polymerization and monomer conversion through real-time FTIR [55-57]. The phase separation kinetics and degree are monitored by reactive light transmittance and dynamic mechanical analysis (DMA). The effects of the additive molecular weight, light intensity and film thickness are determined. The resulting materials are tested in uniaxial tension and compression to determine the effect of phase separation on the stiffness, strength and ductility.

2. Materials and methods

2.1. Materials

An acrylate monomer, pentaerythritol tetraacrylate (PETA, $M_n=352~g/mol$), was purchased from TCI Chemicals. Additionally, a methacrylate diluent, 2-ethylhexyl methacrylate (2-EHMA, $M_n=198~g/mol$), a photoinitiator, diphenyl(2,4,6-trimethylbenzoyl)phosphine oxide (TPO, $M_n=348~g/mol$), and a polymer additive, polypropylene glycol (PPG, $M_n=425,1000,2000,$ and 4000~g/mol) are used, all of which are supplied by Sigma-Aldrich, are used. Gel permeation chromatography (GPC) experiments were performed to validate these molecular weights and the results are shown in Table S1 of the Supplementary Information (S1). Resins containing PPG additive are referred to here as "PE M_n ", (e.

g., PE 425, PE 1000, etc.). The chemical structures of these components are shown in Fig. 1. The ratio of acrylate monomer to methacrylate diluent is 3:1 by weight (PETA:2-EHMA 75:25 by wt%). The photo-initiator is added in powder form at 0.5 wt% and dissolved into the monomer mixture via gentle heating to $\sim\!60$ °C while stirring to create the photo-curable neat resin. The polymer additive is added to this photo-curable resin in an amount of 15 wt% and dissolved via stirring and gentle heating to $\sim\!60$ °C to create phase-separating, photo-curable resins. Resin samples containing polymer additive of different molecular weights are created.

2.2. Custom-built phase separation detection apparatus

Light transmittance was performed using a custom-built light transmission apparatus, Fig. 2a and b, to evaluate the extent of phase separation in the PPG-containing resins. The apparatus includes a S120VC Photodiode Power Sensor (wavelength of absorption = 200-1100 nm, ThorLabs), a LX500 OmniCure portable LED UV-lamp, and the sample compartment. A diffusive glass plate which polarizes the incident beam was also used to provide a uniform intensity of light. Samples are contained between a glass slide and a coverslip, both of which are UV-ozone cleaned to remove any contaminants, using a UVO-Cleaner 342 from Jelight Companies, Inc. Tests were performed using various sample thicknesses, b, of 50, 100, 200, or 300 µm. This parameter is controlled in the state before curing using spacers. Thicknesses were maintained upon complete photopolymerization. Liquid resin is added to the glass slide prepped with spacers as shown in Fig. 2c and a coverslip is gently placed on top. This setup is then placed in the center compartment of the light transmission apparatus. The sample is exposed for 15 min to light of various intensities (5.2, 15, and 36 mW/cm²), while transmittance data collection is performed every 30 ms. If phase separation occurs, the transmission decreases initially due to scattering, and then increases due to TPO consumption. The exposure time to the onset of transmittance reduction is considered the induction time of phase separation. Scattering occurs since the refractive index (RI) of the phase-separated subdomains differs from that of the parent phase (Table S2). Both Rayleigh and Mie scattering may take place caused by phase-separating subdomains of dimensions of tens of nm, or comparable to and larger than the probing radiation wavelength (405 nm), respectively [58]. The reliability of this method and apparatus in identifying phase separation was evaluated in a separate study [59].

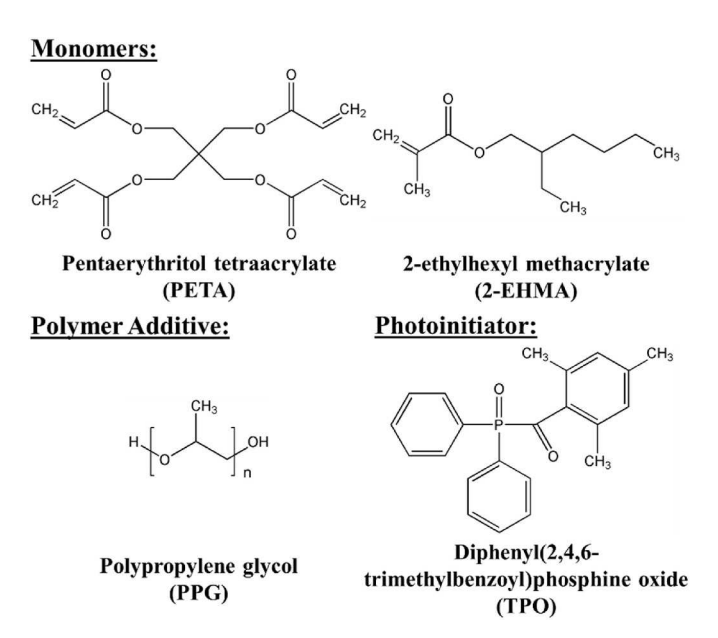


Fig. 1. Chemical structures of monomer components.

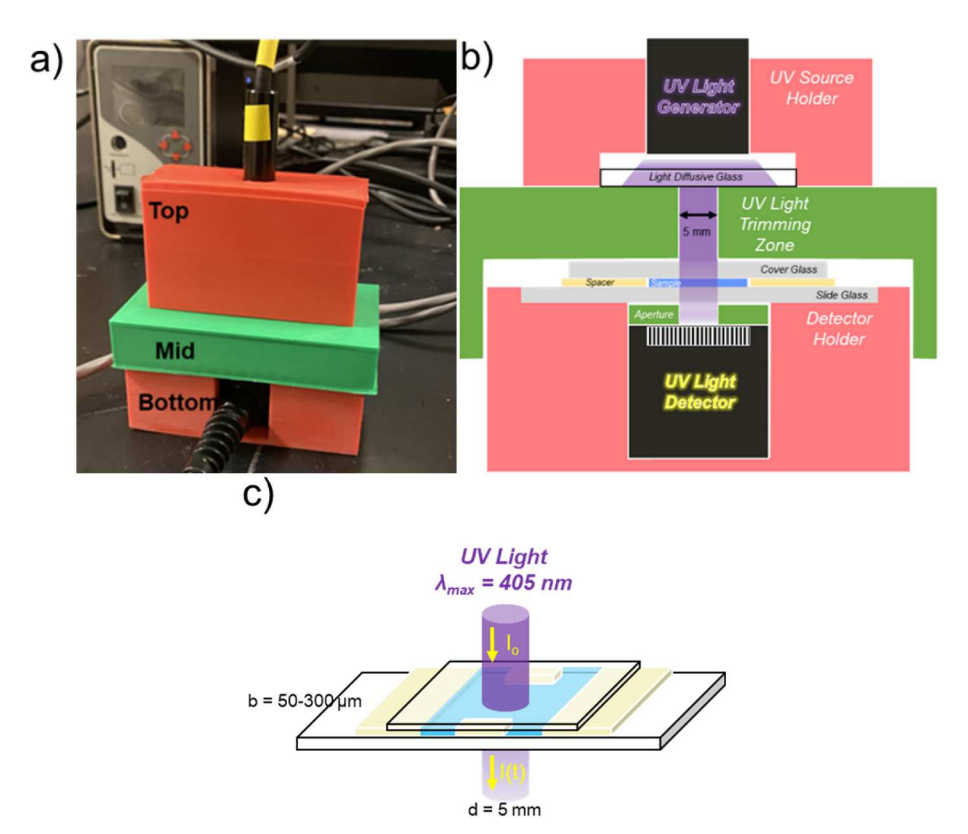


Fig. 2. Custom-built light transmittance apparatus (a) image and (b) schematic. (c) Schematic of sample setup. The path length, 'b,' denotes the film thickness and varies from 50 to 300 μm.

2.3. Material characterization

The monomer conversion and induction time of photopolymerization are determined by real-time FTIR spectroscopy which was performed using a Thermo-Scientific Nicolet iS50 FT-IR equipped with an attenuated total reflectance (ATR) attachment (PIKE Technologies GladiATR). FTIR measurements are performed in the range of wavenumbers from 4000 to 400 cm⁻¹ during resin curing. A LX500 OmniCure portable LED UV-lamp of wavelength 405 nm is used for curing. A 3D-printed part was created to cover the top of the ATR stage and hold the LED UV-lamp to maintain the light dose supplied to the resin sample during the experiment. The light intensity for the FTIR measurement is held constant at 5.2 mW/cm² for the duration of the experiment. Monomer conversion real-time FTIR tests are performed using $100 \mu m$ thick films. A layer of liquid resin is added on top of the ATR crystal and the 3D-printed part holding the LED UV-lamp is positioned over the top. The resin is then cured with light for a duration of 15 min with FTIR data collection occurring every 0.08 s. The conversion is obtained by first acquiring the peak height ratios between two peaks within the Omnic software. The internal reference of the (meth)acrylate carbonyl stretching peak at 1724 cm⁻¹ and the (meth)acrylate alkene -C=C stretching peak at 1635 cm⁻¹ are used, respectively. Within the Omnic software, these ratios are used to calculate and acquire a conversion spectrum in units of absorbance, A. The percent conversion, C, is computed as:

$$C(t)$$
 [%] = $(1 - A(t) / A(0)) \times 100$. (2)

Dynamic mechanical analysis (DMA) was performed using a TA Instruments Discovery DMA 850. Samples were prepared with dimensions $40\times12\times3.2~\text{mm}^3$ using custom-made silicone molds. Glass plates are used to cover the top of the mold and ensure planarity. Samples are then irradiated for 8.5 min at 5.2 mW/cm² light intensity. DMA tests are run at temperatures ranging from $-150~^\circ\text{C}$ to $150~^\circ\text{C}$ with a temperature ramp of 3 $^\circ\text{C/min}$. Liquid nitrogen is used along with a TA Instruments

Gas Cooling Accessory (GCA) to achieve these low temperatures. The single cantilever method is used with an oscillation amplitude of 5 μm and frequency of 1 Hz. The initial preload force is 0.01 N.

To examine the morphologies of polymer films via scanning electron microscopy (SEM), a Versa 3-D Focused Ion Beam - Scanning Electron Microscope (FIB-SEM) by Thermo Fisher Scientific is used. Samples are prepared by first applying a layer of liquid monomer resin to a glass slide with Scotch tape placed as spacers to allow for a uniform thickness of $100 \, \mu m$. This setup is then sandwiched with a coverslip and placed in the light transmission apparatus. The sample is irradiated at a light intensity of 5.2 mW/cm² for 60 s. Following irradiation, films are separated from the glass slide and coverslip using a razor, being mindful of the exposed side. These films are then wiped to remove any residual monomer resin and are placed in a bath of liquid nitrogen for approximately 30 s, removed, and fractured down the center with a razor. The fractured films are washed for 2 min in methanol to remove leftover monomer resin and to dissolve the PPG polymer additive, enabling pore visualization. A piece of double-sided carbon tape is placed on a SEM sample stub. The films are then placed on the tape, with the cross section facing upwards, flush to the edge of the tape. The films are sputter coated with a layer of Au/Pd for a duration of 60 s. Secondary electron images were obtained using an accelerating voltage of 5.0 kV, a working distance of 10 mm, and a beam current of 53 pA. ImageJ software was used to analyze images obtained via SEM to acquire the pore size and pore size distribution.

Uniaxial tension and compression testing are performed with an Instron 5943 equipped with a 1 kN loadcell. Tensile dogbone samples (26 \times 3.2 mm gauge length by width) are prepared using custom-made silicone molds. The planarity of the sample surface is ensured by covering the mold with a glass plate before curing. Samples are tested following standard ASTM638 at a strain rate of 6.4 \times 10 $^{-3}$ s $^{-1}$. Disk-like compression specimens of height 1.6 mm are produced by using an Oring of 3.6 mm inner-diameter as a mold. Samples are subjected to uniaxial compression using the same machine at a strain rate of 1.28 \times

 $10^{-4} \, \mathrm{s}^{-1}$ until rupture or until the upper limit of the load cell is reached. Both compression and tensile tests are performed at room temperature with samples cured for 8.5 min at 5.2 mW/cm² light intensity.

3. Results and discussion

3.1. Effect of sample composition and process parameters on phase separation

The interplay of photopolymerization and phase separation is studied with the transmittance apparatus shown in Fig. 2, which allows exposing samples and measuring their transmittance at the same time. The parameters of the study are the polymer additive molecular weight and the light intensity.

3.1.1. Kinetics and emergence of structure: effect of sample composition and polymer additive molecular weight

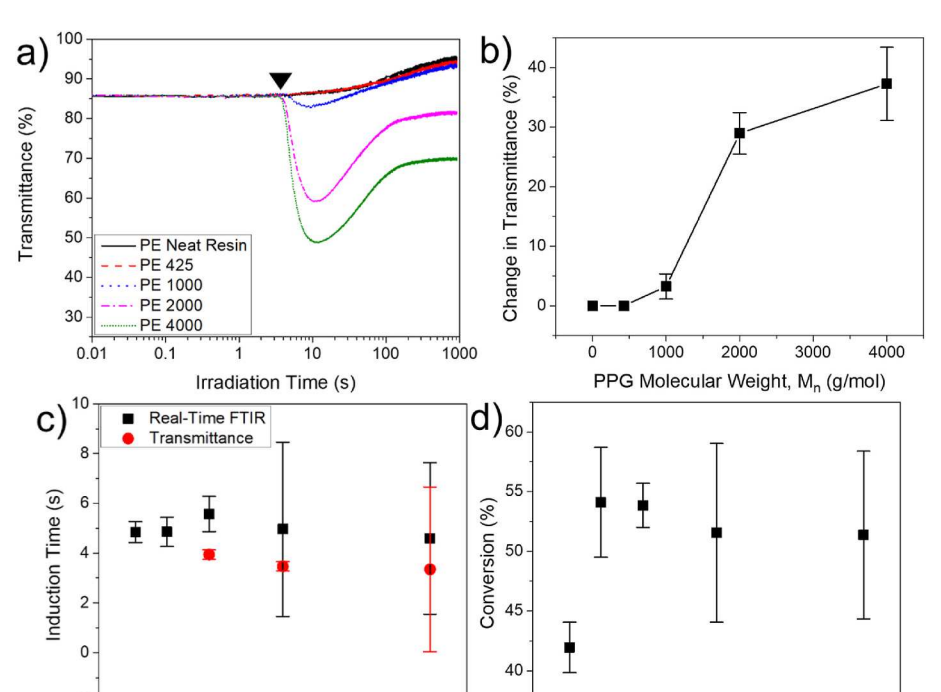
The neat resin and resins containing PPG with various molecular weights, $M_n = 425$, 1000, 2000, and 4000 g/mol, are considered. The variation of transmittance during exposure (light intensity 5.2 mW/cm²) is shown in Fig. 3a. For the neat resin and low M_n resin (PE 425), the only change visible is a slight increase in transmittance throughout the duration of the experiment. This trend is due to the consumption of the photoinitiator, TPO. In resins with $M_n > 1000$, an incubation time of 2–3 s is observed during which the transmittance is constant—regardless of the presence of, or the M_n of the PPG additives. The transmittance decreases rapidly after this stage, which is interpreted as an indication of phase separation. The magnitude of the drop increases with increasing M_n. The transmittance increases again after approximately 10 s of exposure. This recovery is likely due to TPO consumption [60]. In resins with large PPG M_n (PE 2000 and 4000) a plateau in transmittance is seen following the recovery period, where the network and phase separation are believed to have reached thermodynamic equilibrium. The transmittance never fully recovers to the original transmittance prior to photo-polymerization due to the presence of phase-separated subdomains which cause light scattering. In resins with low PPG M_n (PE 425 and 1000), the plateau is not seen. It is believed that in these low

molecular weight systems, smaller subdomains are formed and PPG is partly trapped within the network.

Larger subdomains and more pronounced scattering are expected when the molecular weight of the PPG additive increases. Szczepanski et al. [16] found that photo-PIPS is favored when the polymer additive concentration is larger for low molecular weight additives, while only a small loading level is needed to obtain the same level of phase separation for larger molecular weights. Our results agree with their findings that at a given polymer additive concentration (15 wt% in our case), the photo-PIPS effectiveness increases with increasing PPG molecular weight. This is shown in Fig. 3b where the maximum variation of transmittance from the initial time, t=0 s, to the minimum of the curves in Fig. 3a, $t\sim10$ s, is plotted against the PPG molecular weight.

Phase separation in these systems is driven by the higher hydrophilicity of PPG relative to the developing polymer network. Larger M_n PPG should induce phase separation to a larger extent as the longer chains (larger N at given φ) correspond to a smaller (in absolute value) entropic term in Eq. (1) and hence a larger thermodynamic driving force for separation. Moreover, in systems with larger M_n PPG, the monomers in the photo-curable resin have larger diffusivity relative to PPG. Nevertheless, since all molecular weights of PPG considered are less than the entanglement molecular weight, diffusion of PPG is likely also significant during phase separation [61]. Table S3 shows the viscosities of the pure PPG additives and of the PPG-containing resins. The viscosity varies linearly with Mn for both the pure PPG melts and for the PPG-containing resins before photo-curing, which indicates that both types of systems are unentangled. In the PE 425 system, the driving force of phase separation is smaller and the diffusivities of the resin monomers and PPG molecules are closer to each other. This suggests that a larger probability of PPG entrapment in the developing network exists, which is equivalent to more homogeneously distributed PPG and less phase separation, as indicated by the transmittance data, Fig. 3a. The PE 1000 system shows a situation similar to that observed in the PE 425 case.

The kinetics of phase separation and polymerization processes are compared in Fig. 3c. The induction time of polymerization is determined by real-time FTIR. The data indicates that, within the present accuracy, the induction times are identical and largely independent of PPG M_D.



1000

3000

2000

PPG Molecular Weight, Mn (g/mol)

4000

Fig. 3. (a) Transmittance versus irradiation time for all resin formulations. Samples were irradiated with light intensity 5.2 mW/cm² for 15 min. The arrow indicates the induction time of phase separation. (b) Maximum variation of transmittance (difference between the initial transmittance and the minimum of the curves in (a)) versus PPG molecular weight. (c) Induction times of photopolymerization (obtained from real-time FTIR) compared with the induction time of phase separation (obtained from transmittance). (d) Monomer conversion as obtained from real-time FTIR after 15 min of irradiation. Error bars represent the 95% confidence interval.

2000

PPG Molecular Weight, M_n (g/mol)

1000

This suggests that the onset of measurable phase separation is controlled by the kinetics of the resin monomers at the initial stages of network formation.

In Fig. 3d, the monomer conversion after 15 min of irradiation is shown as a function of PPG M_n . The raw monomer conversion curves are shown in Fig. S1. Conversion is higher in resins with PPG relative to the neat resin. A small decrease of conversion with increasing the PPG M_n is seen in PPG containing resins, Fig. S1. The difference between the resin without PPG and any of the systems containing PPG is interpreted as an indication that PPG separation favors the formation of a more regular network.

To explore the structure of these materials, DMA is performed with samples irradiated to states in the plateau region of Fig. 3a. Fig. 4 shows the storage modulus and $\tan \delta$ curves for all samples. All curves exhibit broad and/or multiple peaks in tan δ . The neat resin shows a broad peak spanning from -26 °C to 56 °C, which indicates that the neat resin network is heterogeneous. Pure poly (PETA) has a T_g of ${\sim}100~^{\circ}\text{C}$ and pure poly (2-EHMA) has a T_g of ~ -10 °C [62,63]. Hence, the broad tan δ peak for the neat resin indicates that phase separation of PETA and 2-EHMA takes place. This is due to the different reactivities of these two components; acrylate monomers react order of magnitude faster than the methacrylates [57,64]. Additionally, since PETA has a high functionality of 4 acrylates per monomer unit, it is likely a fast reacting acrylate. Therefore, in the neat resin system, PETA reacts quickly forcing the 2-EHMA monomers to diffuse away, which leads to regions rich in PETA and others regions rich in 2-EHMA. Further validation of the faster reactivity of PETA versus 2-EHMA is demonstrated in Fig. S2 and Table S4 where it is shown that increasing the PETA fraction in PETA:2-EHMA without PPG leads to smaller induction times for polymerization, but lower overall conversion rates. The networks with increased PETA fraction are expected to be more defective. Note that, in agreement with the observation indicated above that PPG phase separation increases the degree of conversion (Fig. S1), Fig. S2 also indicates that 2-EHMA phase separation increases the overall degree of conversion in PETA:2-EHMA systems.

As PPG is added, further changes of the $\tan\delta$ function are seen. For $M_n=425$ g/mol the $\tan\delta$ peak broadens and shifts to the left. Since the T_g of PPG is approximately -70 °C [65], the shift is associated with the presence of PPG. No clear peak forms though, which indicates that phase separation in this system is not pronounced – as also seen in Fig. 3a – and PPG performs the function of a plasticizer in this case. With increasing the PPG M_n , a clear peak appears in $\tan\delta$ at ~ -60 °C which is associated with the phase separation of PPG. Interestingly, an intermediate peak at ~ -6 °C emerges; this temperature is comparable with the T_g of

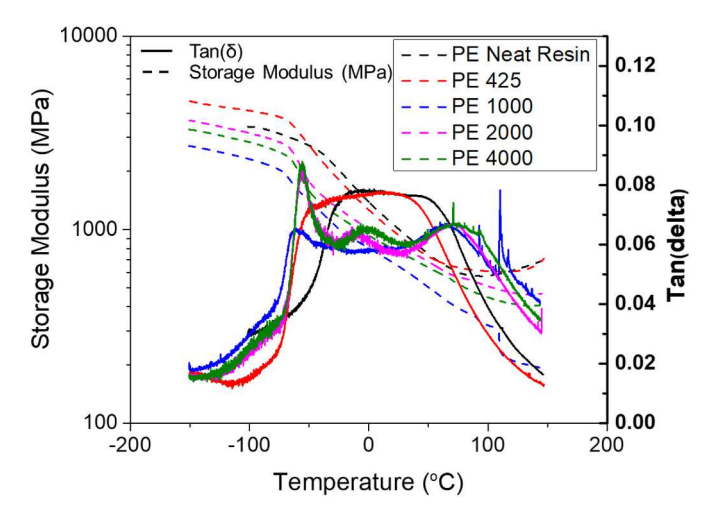


Fig. 4. The storage modulus and $\tan\delta$ curves versus temperature for all resin formulations as determined by DMA analysis. A temperature range of -150 to 150 °C was considered, with a 3 °C/min ramp.

2-EHMA. Most interestingly, the phase separation of 2-EHMA appears to be promoted by the phase separation of PPG, which demonstrates the existence of a synergy between the two processes. Note that the position of the PPG-related peak is identical for PE 2000 and PE 4000, while the 2-EHMA-related peak shifts to lower temperatures (i.e. towards the T_g of pure poly (2-EHMA)) as PPG M_n increases from 2000 to 4000. The material becomes more heterogeneous as the PPG M_n increases and this contributes to reduced transmittance seen in Fig. 3b.

It is interesting to investigate which component of the heterogeneous microstructure, PPG or 2-EHMA subdomains, contributes most to the transmittance reduction. To this end, we analyze the transmittance of neat and PPG-containing films of 50, 100, 200 and 300 μm thickness. Fig. 5a-b shows transmittance versus irradiation time data for the neat and PE 4000 resins, respectively, with various film thicknesses. The overall transmittance decreases for all resins with increasing film thickness, which is expected based on the Beer-Lambert law. For all phase-separating resins (PPG $M_n \geq 1000$), the variation of the transmittance from the initial time, t = 0 s, to the minimum point in the curve (t ~ 10 s), increases with increasing film thickness as shown in Fig. 5c. As the molecular weight of the PPG resins increases, steeper slopes in the variation of transmittance are seen, which is expected due to the increase in phase separation with higher molecular weight of PPG additive. To gain further insight into the process, we assume that the variation of transmittance is due to both absorption and scattering. We write the Beer-Lambert law $T = I_{out}/I_{in} = e^{-ab}$, where T is transmittance, b is the film thickness, and a is the absorption coefficient [66,67]. Considering that the contribution of the two processes (i.e., absorption and scattering) is additive, the following equation can be written,

$$T = e^{-ab} = e^{-a_a b} e^{-a_s b} = T_a T_s \tag{3}$$

Where a_a is the absorption coefficient and a_s is the scattering coefficient. Since at t = 0 s no phase separation is present, $T \sim T_a$. Thus, we use the data at t = 0 s for each resin to evaluate the coefficient a_a . Fig. 5d shows the variation of $-\ln T_{t=0}$ with b for all resin compositions considered. All lines have a similar slope, which indicates that a_a is independent of the sample composition. This is expected since absorption is primarily controlled by the photoinitiator (TPO), which is present at the same concentration in all samples. The intercept of the lines in Fig. 5d decreases slightly with increasing PPG M_n, which indicates the contribution to background absorption of the PPG. Further, we plot the variation of $-\ln T_s = -\ln T/T_{t=0}$ with the film thickness in Fig. 5e and observe that the slope of the curves (i.e., a_s), increases with increasing PPG M_n . Larger a_s implies enhanced scattering due to more pronounced phase separation. With this, it is seen that increased film thickness does not produce larger extents of phase separation. Rather, increasing the film thickness merely increases the amount of light absorption.

The absorption coefficients, a_a , obtained from Fig. 5d and the scattering coefficients, a_s , obtained from Fig. 5e are shown in Fig. 6 for all resin formulations. It is seen that absorption is independent of PPG M_n while scattering increases as M_n increases above $M_n=1000$ g/mol. Scattering is most pronounced in PE 2000 and PE 4000, cases in which both PPG and 2-EHMA phase separate effectively, Fig. 4. However, PPG phase separates in PE 1000 and reaches full separation in PE 2000 and 4000 (the PPG tan δ peaks in these 2 cases are identical), while the 2-EHMA tan δ peak becomes more individualized in PE 2000 and 4000. This correlates with the increase of the scattering coefficient, Fig. 6, suggesting 2-EHMA phase separation is primarily responsible for scattering and the reduction of transmittance shown in Fig. 3a, although PPG phase separation should also play a role.

Direct evidence for phase separation of PPG is obtained by SEM inspection. The samples of Fig. 3a, exposed for 60 s, are processed to remove the PPG content and examined by SEM. Fig. 7a shows the cross-sectional morphologies of these resins. The granularity and size of the voided regions in the cross-sectional area increase with increasing $M_{\rm n}$, showing structure development similar to structures observed by Seo

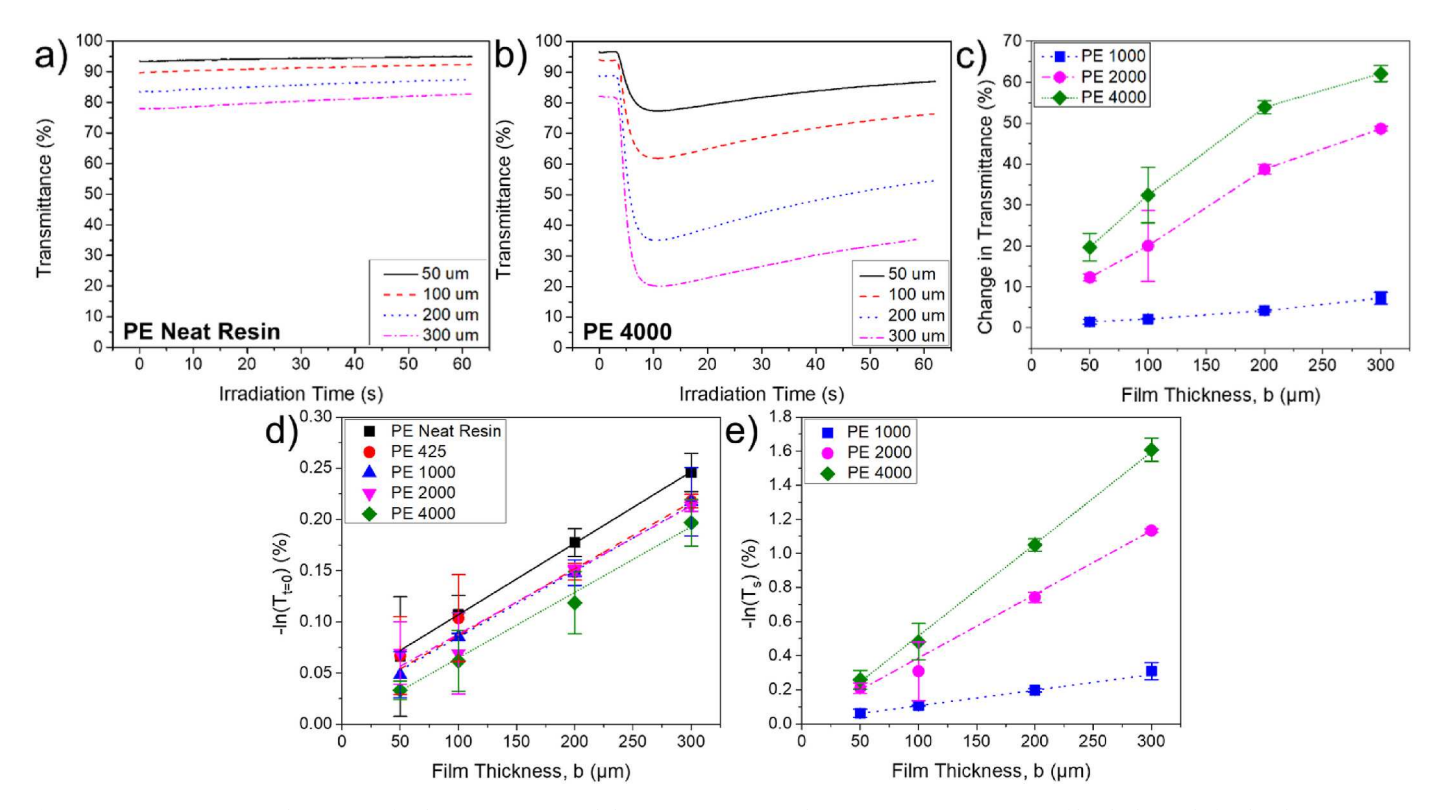


Fig. 5. Transmittance vs. irradiation time for the (a) neat resin and (b) PE 4000 resin. (c) Change in transmittance versus film thickness, b, for the phase-separating resins (PE 1000, 2000, and 4000). (d) Transmission at t = 0 s vs. film thickness for all resins. The slopes indicate the absorption coefficient, a_a , which results identical for all resins, showing that light absorption is independent of the presence of PPG before phase separation. (e) The scattering component of transmittance for each phase-separating resin. The slopes indicate the scattering coefficient, a_s . Larger a_s implies more pronounced phase separation.

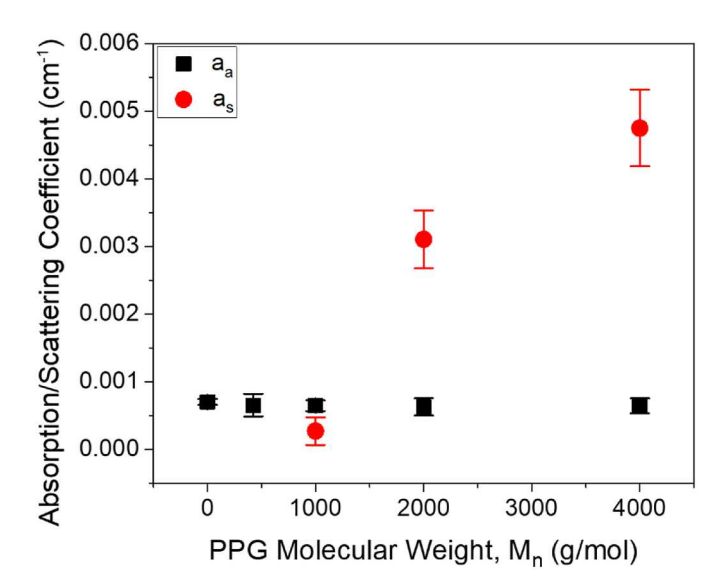


Fig. 6. Variation of absorption and scattering coefficients with the polymer additive molecular weight. Values obtained from Fig. 5d-e.

et al. [40] using styrene-based networks and a PLA-based polymer additive.

Fig. 7b shows the distribution of pore sizes measured in the PE 4000 case, as provided by ImageJ. The distributions for the PE 4000 resin are rather broad and pores of large dimensions, up to 200 nm, exist. The table of Fig. 7c shows the corresponding mean pore diameters and mean network granule diameters of all of the PPG-containing resins. The estimated pore size data suggests the scattering that occurs during the transmittance experiment in the phase-separating resins is

predominantly Rayleigh scattering as the pore sizes are much smaller than the wavelength of light used (405 nm) [58]. We note that the values reported in Fig. 7c represent the size of the intersection of the fracture plane with the PPG subdomains and may be somewhat different from the pore size measured in 3D.

3.1.2. Effect of light intensity

PPG-containing resins are further analyzed via reactive transmittance using various light intensities of 5.2, 15 and 36 mW/cm². Fig. 8a shows transmittance curves for the PE 2000 resin as a function of irradiation time. Similar to Fig. 3, an incubation period is observed initially, after which the induction time of phase separation is seen and transmittance drops. The induction time (indicated by triangles in Fig. 8a) decreases with increasing light intensity since the network forms faster at higher intensities. Fig. 8b shows the induction time plotted against light intensity. It is seen that induction time is not only reduced with an increase in light intensity, but it also is reduced with increasing PPG M_n, as previously confirmed in Fig. 3c. As the light intensity increases, the drop in transmittance decreases, which is indicative of reduced phase separation. With this increasing light intensity, the fastdeveloping polymer network partially entraps the PPG polymer chains restricting complete phase separation from occurring. The trend of decreasing extent of phase separation with increasing light intensity is further demonstrated in Fig. 8c where the change in transmittance is plotted against the PPG molecular weight, with each curve corresponding to a different light intensity. This result agrees with previous findings from Yamashita et al. [44] who demonstrated reduced subdomain sizes with increasing UV or visible light exposure in a PS-PMMA double network, phase-separating system. Similar reduced phase separation has been demonstrated in other systems [15,16,36,39].

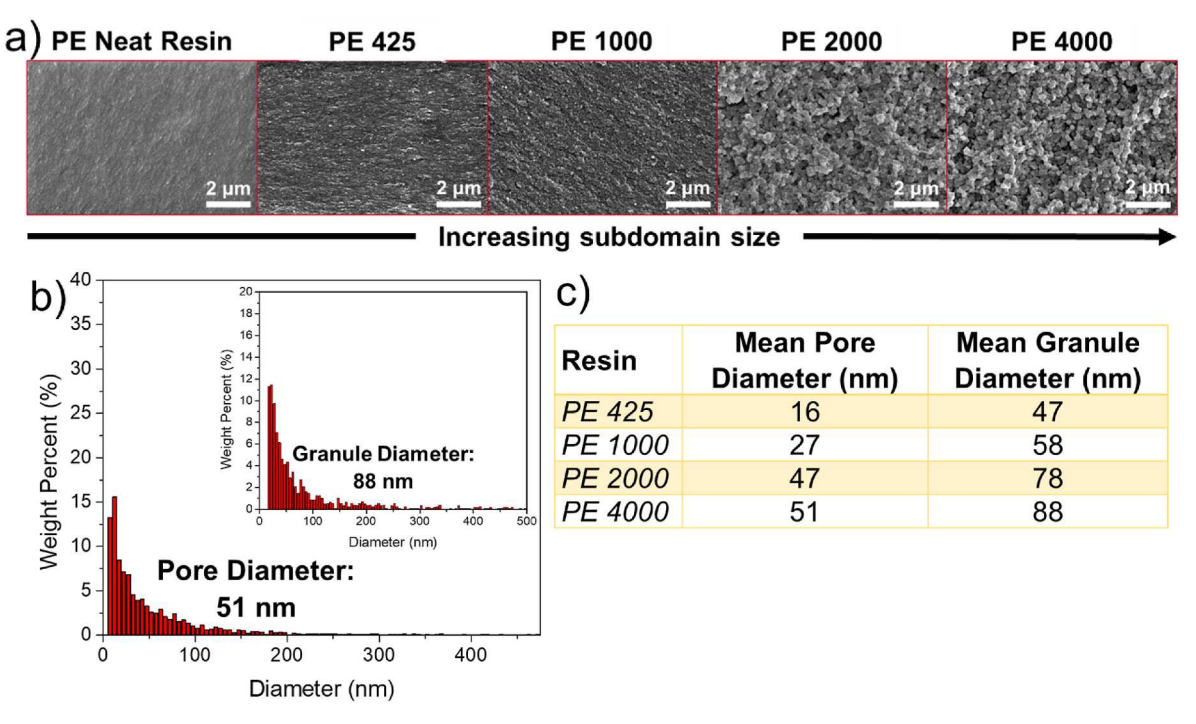


Fig. 7. (a) SEM images of fractured, cross-sectional polymer films at magnification $20,000 \times$ of the various resin formulations. Pores are formed after washing with methanol to remove the phase-separated PPG. (b) Histograms of the mean pore and granule diameters of the PE 4000 resin. (c) Mean pore and granule diameters for all PPG molecular weight resins.

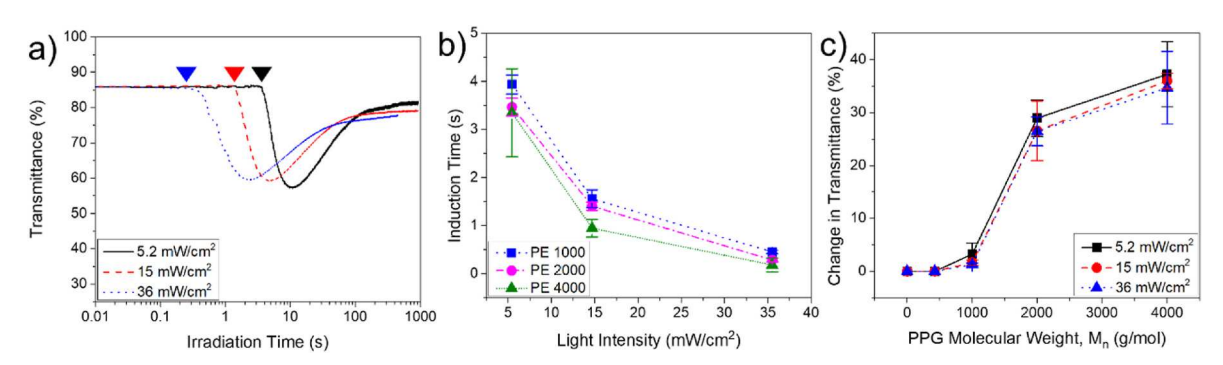


Fig. 8. Variation of transmittance with irradiation time for the (a) PE 2000 resin for light intensities of 5.2, 15, and 36 mW/cm^2 . Arrows indicate the induction time of phase separation. (b) Induction time of phase separation plotted against light intensity for the phase-separating resins: PE 1000, 2000, and 4000. (c) Change in transmittance from the initial time, t = 0 s, to the minimum point of the transmittance curves in (a) versus PPG molecular weight for the three intensities used.

3.2. Mechanical properties characterization

The neat and PPG-containing resins irradiated with light intensity $5.2~\mathrm{mW/cm^2}$ for $8.5~\mathrm{min}$ are subjected to uniaxial compression and tensile testing to evaluate the extent to which PPG phase separation modifies mechanical properties. We note that PPG of all molecular weights considered here is liquid at room temperature and hence the phase-separated subdomains are expected to have lower shear modulus than the neat resin.

Fig. 9a shows representative tensile nominal stress-strain curves for all materials considered. These samples are cured by exposure to light of parameters indicated in the previous paragraph to allow for sufficient curing. The full curing was confirmed using real-time FTIR as discussed in SI section 5 and Fig. S3. The behavior is brittle in all cases, with strains at failure of approximately 2% (Fig. 9b). Young's modulus decreases slightly as phase separation becomes more prominent. This effect is shown in Fig. 9c where Young's modulus is represented versus PPG molecular weight for both tensile and compressive testing. The reduction is expected based on the observation made in the previous

paragraph that the phase-separated PPG subdomains are expected to have lower stiffness than the surrounding resin. The modulus levels off as PPG M_n increases from 2000 to 4000 g/mol, which agrees with the observation in Fig. 7a that the microstructures of PE 2000 and PE 4000 are similar. Another potential effect leading to modulus reduction is the plasticizing contribution of PPG [68]; this is expected to control the difference between the stiffness of the neat resin and the PE 425 case, but be of smaller importance as PPG M_n increases further and PPG phase separates.

4. Conclusion

In this work, photopolymerization-induced phase separation (photo-PIPS) is implemented into a photo-curable multicomponent monomer resin with polymer additive to create a heterogeneous phase-separated polymer network. As the monomer components are polymerized into a thermosetting network, the polymer additive, PPG, as well as the diluent, 2-EHMA, phase separate. It is proved through transmittance, DMA, and SEM analysis that the molecular weight of the polymer

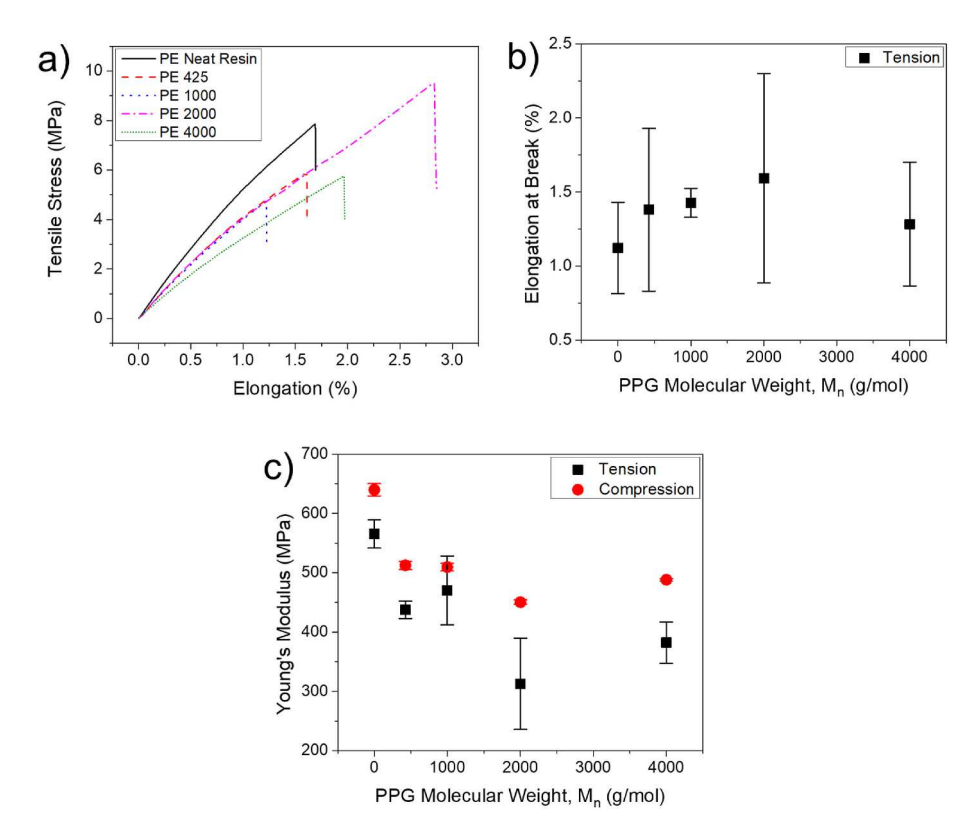


Fig. 9. (a) Representative tensile stress-strain curves. (b) The elongation at break measured in tension. (c) Young's modulus measured in tension and compression for the various resins. Error bars represent the standard error.

additive directly influences the extent of phase separation achievable in the system; not only that the phase separation of PPG becomes more pronounced as PPG Mn increases, but a synergetic effect is observed in that PPG separation favors the phase separation of 2-EHMA. Further validation of this was shown in the film thickness study which implied that scattering was highest in the PE 2000 and 4000 resins. Moreover, when comparing to the DMA analysis, it seems as though scattering is mostly caused by the 2-EHMA subdomains. Light intensity also shows an effect on the extent of phase separation possible within the photocurable resin. With increasing intensity, the extent of phase separation decreases. This is because the rate of phase separation becomes slower than that of photopolymerization. Phase separation leads to a reduction of the material stiffness and strength, while the strain at failure is independent of the degree of phase separation. Through this work, we demonstrate that complex microstructures can be fabricated through the photo-PIPS process which have implications for the mechanical behavior of the material. In particular, some of the methods demonstrated in this work can be used in other systems to fine tune the extent of phase separation and heterogeneity of the network to alter the overall material properties.

CRediT authorship contribution statement

Lauren Zakrzewski: perform experiments, Data curation, write manuscript. **Yeongsik Kim:** Data curation. **Younghan Song:** Data curation. **Chang Y. Ryu:** project coordination, Formal analysis, manuscript writing. **Chulsung Bae:** project coordination, Formal analysis, Writing – original draft. **Catalin R. Picu:** project coordination, Formal analysis, Writing – original draft.

Declaration of competing interest

The authors declare that they have no known competing financial interests or personal relationships that could have appeared to influence the work reported in this paper.

Data availability

Data will be made available on request.

Acknowledgment

This research was supported by the NSF through grant CMMI-2007909.

Appendix A. Supplementary data

Supplementary data to this article can be found online at https://doi.org/10.1016/j.polymer.2023.126032.

References

- H.M.J. Boots, J.G. Kloosterboer, C. Serbutoviez, F.J. Touwslager, Polymerizationinduced phase separation. 1. Conversion-phase diagrams, Macromolecules 29 (1996) 7683–7689.
- [2] C. Serbutoviez, J.G. Kloosterboer, H.M.J. Boots, F.J. Touwslager, Polymerizationinduced phase separation. 2. Morphology of polymer-dispersed liquid crystal thin films, Macromolecules 29 (1996) 7690–7698.
- [3] R.J.J. Williams, B.A. Rozenberg, J.-P. Pascault, Reaction-induced phase separation in modified thermosetting polymers, Adv. Polym. Sci. 128 (1997) 95–156.
- [4] W. Li, L.J. Lee, Low temperature cure of unsaturated polyester resins with thermoplastic additives I. Dilatometry and morphology study, Polymer 41 (2000) 685–696.
- [5] H. Kihara, T. Miura, Morphology of a hydrogen-bonded LC polymer prepared by photopolymerization- induced phase separation under an isotropic phase, Polymer 46 (23) (2005) 10378–10382, https://doi.org/10.1016/j.polymer.2005.08.068.
- [6] S. Park, H.K. Kim, J.W. Hong, Investigation of the photopolymerization-induced phase separation process in polymer dispersed liquid crystal, Polym. Test. 29 (7) (2010) 886–893, https://doi.org/10.1016/j.polymertesting.2010.05.015.
- [7] I.J. Roh, S. Ramaswamy, W.B. Krantz, A.R. Greenberg, Poly(Ethylene chlorotrifluoroethylene) membrane formation via thermally induced phase separation (TIPS), J. Membr. Sci. 362 (1–2) (2010) 211–220, https://doi.org/10.1016/j.memsci.2010.06.042.

- [8] J. Wang, L. Wang, W. Ruan, C. Zhang, J. Ji, Rheology behavior of high-density polyethylene/diluent blends and fabrication of hollow-fiber membranes via thermally induced phase separation, J. Appl. Polym. Sci. 118 (4) (2010) 2186–2194, https://doi.org/10.1002/app.32584.
- [9] Y. Zhang, F. Chen, W. Shi, Y. Liang, C.C. Han, Layered structure formation in the reaction-induced phase separation of epoxy/polysulfone blends, Polymer 51 (25) (2010) 6030–6036, https://doi.org/10.1016/j.polymer.2010.10.027.
- [10] C. Zhang, Y. Bai, Y. Sun, J. Gu, Y. Xu, Preparation of hydrophilic HDPE porous membranes via thermally induced phase separation by blending of amphiphilic PEb-PEG copolymer, J. Membr. Sci. 365 (1–2) (2010) 216–224, https://doi.org/ 10.1016/j.memsci.2010.09.007.
- [11] M.W. Schulze, L.D. McIntosh, M.A. Hillmyer, T.P. Lodge, High-modulus, high-conductivity nanostructured polymer electrolyte membranes via polymerization-induced phase separation, Nano Lett. 14 (1) (2014) 122–126, https://doi.org/10.1021/pil4034818.
- [12] D.M. Smith, C.Y. Li, T.J. Bunning, Light-directed mesoscale phase separation via holographic polymerization, J. Polym. Sci. B Polym. Phys. 52 (3) (2014) 232–250, https://doi.org/10.1002/polb.23413.
- [13] A.H. Torbati, H.B. Nejad, M. Ponce, J.P. Sutton, P.T. Mather, Properties of triple shape memory composites prepared via polymerization-induced phase separation, Soft Matter 10 (17) (2014) 3112–3121, https://doi.org/10.1039/c3sm52599f.
- [14] R.J.J. Williams, C.E. Hoppe, I.A. Zucchi, H.E. Romeo, I.E. dell'Erba, M.L. Gómez, J. Puig, A.B. Leonardi, Self-assembly of nanoparticles employing polymerizationinduced phase separation, J. Colloid Interface Sci. 431 (2014) 223–232, https:// doi.org/10.1016/j.jcis.2014.06.022.
- [15] C.R. Szczepanski, J.W. Stansbury, Accessing photo-based morphological control in phase-separated, cross-linked networks through delayed gelation, Eur. Polym. J. 67 (2015) 314–325, https://doi.org/10.1016/j.eurpolymj.2015.04.006.
- [16] C.R. Szczepanski, J.W. Stansbury, Modification of linear prepolymers to tailor heterogeneous network formation through photo-initiated polymerization-induced phase separation, Polymer 70 (2015) 8–18, https://doi.org/10.1016/j. polymer.2015.06.002.
- [17] E. Kemiklioglu, L.C. Chien, Effects of photoinitiator on electro-optical properties of polymerization-induced phase separation blue-phase liquid crystals, European Physical Journal E 40 (4) (2017), https://doi.org/10.1140/epje/i2017-11524-6.
- [18] S. Guo, G. Kang, D.T. Phan, M.N. Hsu, Y.C. Por, C.H. Chen, Polymerization-induced phase separation formation of structured hydrogel particles via microfluidics for scar therapeutics, Sci. Rep. 8 (1) (2018), https://doi.org/10.1038/s41598-018-20516-9
- [19] Y. Ding, Q. Zhao, L. Wang, L. Huang, Q. Liu, X. Lu, Y. Cai, Polymerization-induced self-assembly promoted by liquid-liquid phase separation, ACS Macro Lett. 8 (8) (2019) 943–946, https://doi.org/10.1021/acsmacrolett.9b00435.
- [20] P. Zhang, D.C. Sundberg, J.G. Tsavalas, Polymerization induced phase separation in composite latex particles during seeded emulsion polymerization, Ind. Eng. Chem. Res. 58 (2019) 21118–21129, https://doi.org/10.1021/acs.iecr.9b02964.
 [21] P. Zhang, Z. Gao, Q. Zhang, A. Khattab, G. Li, Fracture behavior characterization of
- [21] P. Zhang, Z. Gao, Q. Zhang, A. Khattab, G. Li, Fracture behavior characterization of arcan polycaprolactone based polymer composites prepared by polymerization induced phases separation, Polym. Compos. 40 (3) (2019) 1198–1208, https://doi. org/10.1002/pc.24831.
- [22] C. Kahrs, T. Gühlstorf, J. Schwellenbach, Influences of different preparation variables on polymeric membrane formation via nonsolvent induced phase separation, J. Appl. Polym. Sci. 137 (28) (2020), https://doi.org/10.1002/ app_48852
- [23] M. Pavlovic, M. Antonietti, B.V.K.J. Schmidt, L. Zeininger, Responsive janus and cerberus emulsions via temperature-induced phase separation in aqueous polymer mixtures, J. Colloid Interface Sci. 575 (2020) 88–95, https://doi.org/10.1016/j. ipic.2020.04.067
- [24] A. Sellinger, P.M. Weiss, A. Nguyen, Y. Lu, R.A. Assink, W. Gong, C.J. Brinker, Continuous self-assembly of organic-inorganic nanocomposite coatings that mimic nacre, Nature 394 (1998) 256–260.
- [25] H. Gao, B. Ji, I.L. Jäger, E. Arzt, P. Fratzl, Materials become insensitive to flaws at nanoscale: lessons from nature, Proc. Natl. Acad. Sci. USA 100 (10) (2003).
- [26] S. Weiner, H.D. Wagner, The material bone: structure-mechanical function relations, Annu. Rev. Mater. Sci. 28 (1998) 271–298.
- [27] M.A. Meyers, A.Y.M. Lin, P.Y. Chen, J. Muyco, Mechanical strength of abalone nacre: role of the soft organic layer, J. Mech. Behav. Biomed. Mater. 1 (1) (2008) 76–85, https://doi.org/10.1016/j.jmbbm.2007.03.001.
- [28] J.D. Currey, Mechanical properties of mother of pearl in tension, Proc. R. Soc. Lond. B Biol. Sci. 196 (1125) (1977) 443–463, https://doi.org/10.1098/ rspb.1977.0050.
- [29] J.D. Currey, J.D. Taylor, The mechanical behaviour of some Molluscan hard tissues. J. Zool. 173 (3) (1974) 395–406.
- [30] A.P. Jackson, J.F.V. Vincent, R.M. Turner, The mechanical design of nacre, Proc. R. Soc. Lond. B Biol. Sci. 234 (1277) (1988) 415–440, https://doi.org/10.1098/rspb.1988.0056.
- [31] P.M. Lipic, F.S. Bates, M.A. Hillmyer, Nanostructured thermosets from selfassembled amphiphilic block copolymer/epoxy resin mixtures, J. Am. Chem. Soc. 120 (1998) 8963–8970.
- [32] J.D. Clapper, J.M. Skeie, R.F. Mullins, C.A. Guymon, Development and characterization of photopolymerizable biodegradable materials from PEG-PLA-PEG block macromonomers, Polymer 48 (22) (2007) 6554–6564, https://doi.org/ 10.1016/j.polymer.2007.08.023.
- [33] A. Bonnet, J.P. Pascault, H. Sautereau, M. Taha, Y. Camberlin, Epoxy-diamine thermoset/thermoplastic blends. 1. Rates of reactions before and after phase separation, Macromolecules 32 (25) (1999) 8517–8523, https://doi.org/10.1021/ ma981754p.

- [34] R.C. Willemse, E.J.J. Ramaker, J. van Dam, A. Posthuma De Boer, Morphology development in immiscible polymer blends: initial blend morphology and phase dimensions, Polymer 40 (1999) 6651–6659.
- [35] H. Veenstra, J. van Dam, A. Posthuma De Boer, On the coarsening of Co-continuous morphologies in polymer blends: effect of interfacial tension, viscosity and physical cross-links, Polymer 41 (2000) 3037–3045.
- [36] K. Murata, J. Sachin, H. Etori, T. Anazawa, Photopolymerization-induced phase separation in binary blends of photocurable/linear polymers, Polymer 43 (2002) 2845–2859
- [37] Y. Sasaki, N. Aiba, H. Hashimoto, J. Kumaki, Reversible hierarchical phase separation of a poly(methyl methacrylate) and poly(n-nonyl acrylate) blend in a Langmuir monolayer, Macromolecules 43 (21) (2010) 9077–9086, https://doi. org/10.1021/ma102027t.
- [38] N. Naderi, S. Rastegar, M. Mohseni, M. Khorasani, Controlling final morphologies of two-step polymerization induced phase separated blends of trimethylolpropane triacrylate/acrylate copolymer through copolymer molecular weight, Polym. Test. 61 (2017) 146–149, https://doi.org/10.1016/j.polymertesting.2017.04.002.
- [39] N. Naderi, S. Rastegar, M. Mohseni, M. Khorasani, Photo-polymerization induced viscoelastic phase separation of trimethylolpropane triacrylate/poly (styrene-Comethyl methacrylate) blends, Polymer 153 (2018) 391–397, https://doi.org/ 10.1016/j.polymer.2018.03.038.
- [40] M. Seo, M.A. Hillmyer, Reticulated nanoporous polymers by controlled polymerization-induced microphase separation, Science 336 (6087) (2012) 1422–1425, https://doi.org/10.1126/science.1221383, 1979.
- [41] A. Hara, R. Inoue, N. Takahashi, K. Nishida, T. Kanaya, Trajectory of critical point in polymerization-induced phase separation of epoxy/oligoethylene glycol solutions, Macromolecules 47 (13) (2014) 4453–4459, https://doi.org/10.1021/ ma5009258.
- [42] W. Wang, Y. Pan, K. Shi, C. Peng, X. Ji, Hierarchical porous polymer beads prepared by polymerization-induced phase separation and emulsion-template in a microfluidic device, Chin. J. Polym. Sci. 32 (12) (2014) 1646–1654, https://doi. org/10.1007/s10118-014-1547-1.
- [43] X. Yi, L. Kong, X. Dong, X. Zuo, X. Kuang, Z. Feng, D. Wang, Polymerization induced viscoelastic phase separation of porous phenolic resin from solution, Polym. Int. 65 (9) (2016) 1031–1038, https://doi.org/10.1002/pi.5147.
- [44] Y. Yamashita, K. Komori, T. Murata, H. Nakanishi, T. Norisuye, T. Yamao, Q. Tran-Cong-Miyata, Conducting polymer networks synthesized by photopolymerization-induced phase separation, Adv. Nat. Sci. Nanosci. Nanotechnol. 9 (1) (2018), https://doi.org/10.1088/2043-6254/aaabae.
- [45] D.G. Moore, L. Barbera, K. Masania, A.R. Studart, Three-dimensional printing of multicomponent glasses using phase-separating resins, Nat. Mater. 19 (2) (2020) 212–217, https://doi.org/10.1038/s41563-019-0525-y.
- [46] Y. Tang, K. Wu, S. Yu, J. Chen, X. Ding, L. Rao, Z. Li, Bioinspired high-scattering polymer films fabricated by polymerization-induced phase separation, Opt Lett. 45 (10) (2020), https://doi.org/10.1364/ol.390639, 2918–1921.
- [47] F. Wang, L. Ratke, H. Zhang, P. Altschuh, B. Nestler, A phase-field study on polymerization-induced phase separation occasioned by diffusion and capillary flow—a mechanism for the formation of porous microstructures in membranes, J. Sol. Gel Sci. Technol. 94 (2) (2020) 356–374, https://doi.org/10.1007/s10971-020-05238-7
- [48] P.K. Chan, A.D. Rey, Polymerization-induced phase separation. 1. Droplet size selection mechanism, Macromolecules 29 (1996) 8934–8941.
- [49] T.-S. Chung, The limitations of using flory-huggins equation for the states of solutions during asymmetric hollow-fiber formation, J. Membr. Sci. 126 (1997) 19–34
- [50] P.K. Chan, A.D. Rey, Polymerization-induced phase separation. 2. Morphological analysis, Macromolecules 30 (1997) 2135–2143.
- [51] F.P.W. Melchels, J. Feijen, D.W. Grijpma, A review on stereolithography and its applications in biomedical engineering, Biomaterials 31 (24) (2010) 6121–6130, https://doi.org/10.1016/j.biomaterials.2010.04.050.
- [52] M. Hofmann, 3D printing gets a boost and opportunities with polymer materials, ACS Macro Lett. 3 (4) (2014) 382–386, https://doi.org/10.1021/mz4006556.
- [53] S.C. Ligon, R. Liska, J. Stampfl, M. Gurr, R. Mülhaupt, Polymers for 3D printing and customized additive manufacturing, Chem. Rev. 117 (15) (2017) 10212–10290, https://doi.org/10.1021/acs.chemrev.7b00074.
- [54] J. Yao, M. Takahashi, T. Yoko, Controlled preparation of macroporous TiO2 films by photo polymerization-induced phase separation method and their photocatalytic performance, Thin Solid Films 517 (24) (2009) 6479–6485, https://doi.org/10.1016/j.tsf.2009.03.214.
- [55] J. v Crivello, Synergistic effects in hybrid free radical/cationic photopolymerizations, J. Polym. Sci. Polym. Chem. 45 (16) (2007) 3759–3769, https://doi.org/10.1002/pola.22126.
- [56] E. Andrzejewska, Photopolymerization kinetics of multifunctional monomers, Prog. Polym. Sci. 26 (2001) 605–665.
- [57] S. Beuermann, M. Buback, Rate coefficients of free-radical polymerization deduced from pulsed laser experiments, Prog. Polym. Sci. 27 (2002) 191–254.
- [58] J. Beyerer, F. Puente León, C. Frese, Machine Vision Automated Visual Inspection: Theory, Practice and Applications, first ed., Springer-Verlag, Berlin, Heidelberg, 2016 https://doi.org/10.1007/978-3-662-47794-6.
- [59] Y. Kim, Y. Song, C.Y. Ryu, C. Bae, C.R. Picu, Reactive UV transmittance analysis in photopolymerization induced phase separation, 2023 in preparation.
- [60] L. Zakrzewski, Y. Kim, Y. Song, C.Y. Ryu, C. Bae, C.R. Picu, Competition between Phase Separation and Photopolymerization Kinetics during Polymeric Network Development, 2023 in preparation.

- [61] K.L. Ngai, A. Schónhals, E. Schlosser, An explanation of anomalous dielectric relaxation properties of polypropylene glycol), Macromolecules 25 (1992) 4015–4010.
- [62] IGM Resins, Energy curing product guide. https://www.igmresins.com/Product_d ocumentation/IGM_General_Product_Guide_4_5_Digital.pdf. (Accessed 30 April 2023)
- [63] Jamorin International, 2-Ethylhexyl methacrylate F (2-EHMA F). https://jamorin.com/products/2-ethylhexyl-methacrylate-2-ehma/. (Accessed 30 April 2023).
- [64] H. Kilambi, J.W. Stansbury, C.N. Bowman, Enhanced reactivity of monovinyl acrylates characterized by secondary functionalities toward photopolymerization and michael addition: contribution of intramolecular effects, J. Polym. Sci. Polym. Chem. 46 (10) (2008) 3452–3458.
- [65] M. Tarnacka, A. Talik, E. Kamińska, M. Geppert-Rybczyńska, K. Kaminski, M. Paluch, The impact of molecular weight on the behavior of poly(propylene glycol) derivatives confined within alumina templates, Macromolecules 52 (9) (2019) 3516–3529, https://doi.org/10.1021/acs.macromol.9b00209.

Polymer 280 (2023) 126032

- [66] I. Oshina, J. Spigulis, Beer–lambert law for optical tissue diagnostics: current state of the art and the main limitations, J. Biomed. Opt. 26 (10) (2021), https://doi. org/10.1117/1.jbo.26.10.100901.
- [67] R.I. Barbosa, E.C. de O. Guirro, L. Bachmann, H.E. Brandino, R.R. de J. Guirro, Analysis of low-level laser transmission at wavelengths 660, 830 and 904 Nm in biological tissue samples, J. Photochem. Photobiol., B 209 (2020), https://doi.org/ 10.1016/j.jphotobiol.2020.111914.
- [68] V. Marturano, P. Cerruti, V. Ambrogi, Polymer additives, Physical Sciences Reviews 2 (6) (2019), https://doi.org/10.1515/psr-2016-0130.